Available online at www.sciencedirect.com
ScienceDirect
Proceedings of the Combustion Institute 31 (2007) 765–773
Proceedings of the Combustion Institute
www.elsevier.com/locate/proci

Quantitative laser-induced fluorescence measurements of nitric oxide in a heavy-duty Diesel engine

K. Verbiezen [a], R.J.H. Klein-Douwel [b], A.P. van Vliet [a], A.J. Donkerbroek [a], W.L. Meerts [a], N.J. Dam [a,*], J.J. ter Meulen [a]

[a] *Applied Molecular Physics, Institute for Molecules and Materials, Radboud University Nijmegen, Toernooiveld 1, 6525 ED Nijmegen, The Netherlands*

[b] *Mechanical Engineering, Eindhoven University of Technology, P.O. Box 513, 5600 MB Eindhoven, The Netherlands*

Abstract

We present quantitative, in-cylinder, UV-laser-induced fluorescence measurements of nitric oxide in a heavy-duty Diesel engine. Processing of the raw fluorescence signals includes a detailed correction, based on additional measurements, for the effect of laser beam and fluorescence attenuation, and for the pressure and temperature dependence of the fluorescence efficiency, based on numerical modelling. These corrections are largest early in the stroke, when quenching rates are high and UV transmission is low. Together, they vary over more than three orders of magnitude during the combustion stroke. Fully quantitative results are realised by an overall calibration using independent concentration measurements in the exhaust gas. The data provide evidence of NO formation during both the premixed and mixing-controlled combustion phases.

Keywords: Nitric oxide; Laser-induced fluorescence; Diesel engine; UV absorption

1. Introduction

Reduction of nitrogen oxides (NO_x) emissions from Diesel engines requires fundamental knowledge of the formation processes involved. Numerical models describing the complex chemistry and fluid dynamics of Diesel combustion are important for the efficient evaluation of new engine designs. These models should be validated with experimental results obtained under characteristic engine conditions. To this end, laser techniques are frequently used, offering robust and non-intrusive diagnostics for measurements at high spatial and temporal resolution.

Although laser-induced fluorescence (LIF) has often been employed for visualisation of nitric oxide (NO) in Diesel engines [1–7] and SI engines [8–14], quantification of the LIF signals in terms of NO densities or mole fractions has proven to be very difficult, requiring (1) knowledge of the (local) excitation laser intensity, (2) knowledge of the attenuation of the ensuing NO fluorescence, and (3) a good spectroscopic model predicting the dependence of NO LIF on temperature, pressure, and gas composition. Finally, the local temperature needs to be known.

* Corresponding author. Fax: +31 24 3653311.
E-mail address: n.dam@science.ru.nl (N.J. Dam).

1540-7489/$ - see front matter © 2006 The Combustion Institute. Published by Elsevier Inc. All rights reserved.
doi:10.1016/j.proci.2006.07.061

In this paper, we present quantitative, crank-angle resolved NO LIF measurements in a Diesel engine by means of A–X (0,0) excitation at 226 nm. Correction strategies for laser beam and fluorescence attenuation are discussed extensively in a separate paper [15], but will be briefly summarised here. We compare the pressure and temperature dependence of NO LIF as predicted by LIFSim [16] to our calculations, with special attention to the influence of the gas composition.

2. NO LIF signal dependence

The fluorescence intensity is determined by a number of (pressure and temperature dependent) factors. Generally, for a laser-induced $i \rightarrow j$ transition, the fluorescence signal from state j to k can be modelled (in the weak excitation limit) as

$$S_{\mathrm{LIF}}^{(k)} \propto N_{\mathrm{NO}} I_{\mathrm{laser}} \tau_{\mathrm{F}} f_{\mathrm{B}} g(\nu_{\mathrm{L}}, \nu_{ij}) \times B_{ij} \frac{A_{jk}}{\sum_l A_{jl} + Q_j}, \tag{1}$$

where N_{NO} is the NO number density in the laser probe volume, I_{laser} the local laser intensity, and τ_{F} the fluorescence transmission on its way to the detector. $f_{\mathrm{B}}(T)$ is the Boltzmann fraction, $g(\nu_{\mathrm{L}},\nu_{ij})$ the overlap integral of the laser spectral profile and the absorption line, and B_{ij} the Einstein coefficient for absorption on this transition. The fraction at the right is known as the Stern-Vollmer factor, and is the ratio of the fluorescence rate (i.e. the Einstein coefficient for spontaneous emission A) to the total decay rate, including other fluorescent transitions and non-radiative collisional energy transfer (rate constant Q). Since pressure broadening and collisional quenching are species dependent, evaluation of Eq. (1) depends on the gas composition. Results may be presented in terms of number densities, N_{NO}, or mole fraction, χ_{NO}, related by

$$\chi_{\mathrm{NO}} = \frac{N_{\mathrm{NO}}}{N_{\mathrm{total}}} = N_{\mathrm{NO}} \frac{k_{\mathrm{B}} T_{\mathrm{probe}}}{p}, \tag{2}$$

with N_{total} the total number density, k_{B} Boltzmann's constant, T_{probe} the local temperature, and p the pressure.

3. Experiment

3.1. The engine

The optical engine is a heavy-duty, six-cylinder Diesel engine; specifications are listed in Table 1. Figure 1 shows the optically accessible measurement cylinder.

A slot machined into the piston crown allows observations through one of the side windows

Table 1
Engine specifications and operating conditions

Engine type	Four-stroke, DI Diesel engine
Bore	130 mm
Stroke	146 mm
Displacement	1.939 ℓ
Compression ratio	15 (unmodified: 16)
Swirl number	1.8
Fuel injected	60 mg city Diesel
Boost pressure	1.4 bar (abs.; no EGR)
Speed/gIMEP	1430 rpm/500 kPa

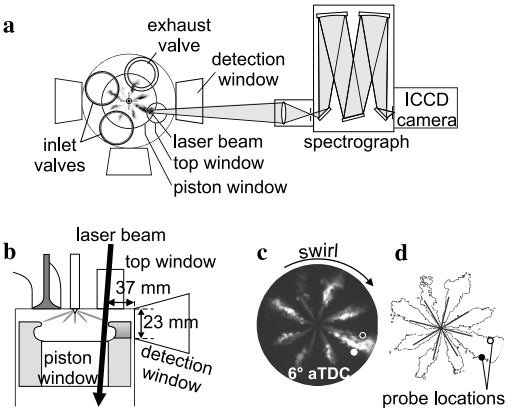

Fig. 1. Schematic representation of the setup: (a) top view; (b) close-up side view of the measurement cylinder; (c) 100 ns snapshot of the combusting fuel sprays; (d) contour plot of the same image, indicating the two laser probe positions and the spray axes (solid grey lines). The laser beam traverses the cylinder almost parallel to its axis. NO fluorescence is detected by an imaging grating spectrograph via the nearest side window.

even at top dead centre (TDC). The (cam-driven) fuel injection takes place through a central, eight-hole nozzle. The injector can be rotated, allowing measurements at different positions relative to the fuel sprays without repositioning the laser beam. To avoid overheating the non-lubricated measurement cylinder is skip-fired. Steady-state conditions are mimicked by (pre-)heating the cooling water to operational temperatures.

Figure 2 shows some characteristics for the measurement cylinder. The heat release rate shows that combustion begins around 3° after TDC (aTDC).

3.2. NO LIF experiments

All measurements have been carried out with the laser beam traversing the combustion chamber parallel to the cylinder axis, probing either *through* a fuel spray or exactly *between* two sprays

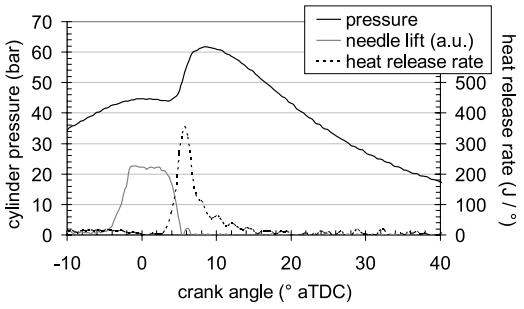

Fig. 2. Cylinder pressure, heat release rate, and needle lift (in arbitrary units) for the engine conditions relevant here.

(indicated in Fig. 1d). NO LIF is induced by laser radiation at 226.03 nm, resonant with the coinciding $A^2\Sigma(v'=0) \leftarrow X^2\Pi(v''=0)$ $P_1(23.5)$, $Q_1 + P_{21}(14.5)$, and $Q_2 + R_{12}(20.5)$ transitions. Laser radiation is produced by a frequency-mixed dye laser (Radiant Narrowscan D, using Rhodamin 101) pumped by a seeded Nd:YAG laser (Continuum Powerlite Precision II 8010). The unfocussed beam (~3.5 mm diameter) of 5 mJ pulse energy is directed into the combustion chamber via the top window, immediately entering the field of view. Four vibronic fluorescence bands (at 237, 248, 259, and 270 nm, corresponding to the A–X (0,1)–(0,4) transitions, respectively) are detected through the nearest side window by an intensified CCD camera (Roper Scientific, ICCD 512T, 512^2 pixels, 16 bits) mounted behind a spectrograph (ARC SpectraPro 500i, 600 lines/mm grating). The entrance slit of the spectrograph is parallel to the laser beam direction, and fully opened for maximum signal. Elastic scattering is suppressed by a 0° 226-nm mirror. In this configuration, the path lengths of laser beam and fluorescence within the combustion chamber are kept minimal (23 and 37 mm, respectively), thereby minimising the effect of attenuation.

Fluorescence imaging through a grating spectrograph is advantageous for a number of reasons. First, it allows correction for any broadband background signal (which was found negligible in our measurements). Second, interference of LIF from O_2 molecules can be monitored (found to be minimal in our experiments). Thirdly, since the spectrograph provides NO fluorescence images for each vibronic emission band individually, variations in relative band intensities throughout the stroke can be used to derive effective attenuation coefficients [15], as will be described in more detail below. As a disadvantage, imaging through a grating spectrograph degrades spatial resolution. If desired, this can be compensated for to a large extent by proper post-processing [17,18], but that is not pursued here.

3.3. Attenuation measurements

Ideally, all attenuation correction experiments (detailed below) are performed simultaneously with the NO LIF measurements. Due to practical reasons this was not feasible in our setup (except for the attenuation assessments that are based on the NO LIF spectrum itself, see Section 4.2). As a consequence, we correct cycle-averaged NO measurements with cycle-averaged attenuation factors. Of course, the engine conditions and the two laser probe locations were kept identical for all measurements.

3.4. Calibration

The NO LIF measurements are calibrated by scaling the in-cylinder concentration curve (still in arbitrary units) such that its value at the end of the stroke (the exhaust valve opens at 130° aTDC) matches the exhaust NO concentration, as determined by a commercial exhaust gas analyser (SIGNAL Instruments, NOX analyser series 4000). The latter is connected to the exhaust of only the measurement cylinder; its reading is scaled by the skip-fire ratio. We assume reasonably homogeneous NO distributions at 130° aTDC.

4. Data processing

4.1. Interpretation of NO LIF images

Two example NO LIF images are shown in Fig. 3, for 8° and 130° aTDC. The vertical axis displays spatial information (parallel to the laser beam); wavelength dispersion is in the horizontal direction. If the entrance slit of the spectrograph were narrow, one would obtain a pure spectrum. In our case (open slit), the spectra are convolved with the spatial intensity profile of the laser beam and the NO density. Still, the vibronic fluorescence bands are clearly separated. They are labelled by transition and wavelength in Fig. 3.

At 8° aTDC, the field of view is limited by the piston blocking the lower part of the detection window, causing an apparently shorter NO image. The window is clear from 27° aTDC onwards. The examples in Fig. 3 show that, in our case, both O_2 interference and broadband background luminescence (i.e. laser-induced incandescence, fuel LIF) are negligible with 226 nm excitation, although some broadband (fuel) LIF can be observed at the "through spray" position shortly after TDC (not shown).

The NO measurements presented in this work are spatially averaged spectra, obtained by summing all pixel values attributed to individual fluorescence bands within the CCD image, corrected for background. This basically treats the NO

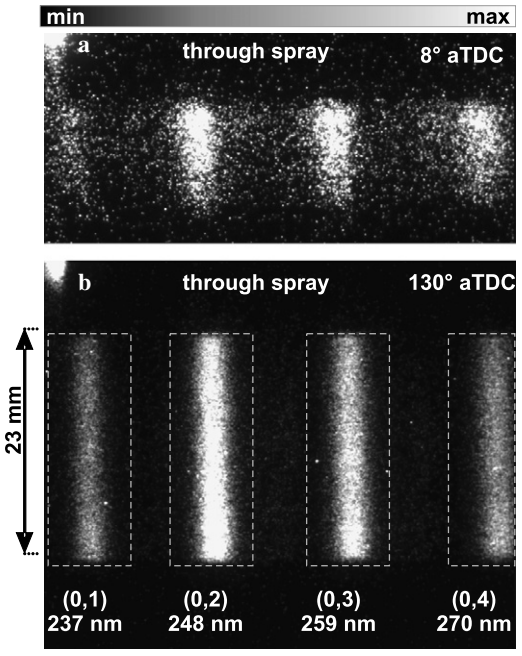

Fig. 3. Two single-shot NO LIF images, recorded at 8° aTDC (a) and 130° aTDC (b). The intensity scales are adjusted to show maximum contrast for each image. The regions of interest for the emission bands are indicated by dashed grey rectangles in (b). The difference in the *relative* peak intensities between the two LIF spectra is attributed to wavelength dependent fluorescence absorption by CO_2 and O_2. This absorption is weaker at 130° aTDC due to the lower temperature. The bright spot in the upper left corner is a reflection of a fraction of the laser beam that was coupled out to monitor pulse-to-pulse energy fluctuations.

LIF data as point measurements, sacrificing the vertical information for clarity (e.g. easy comparison of measurements at different crank angles or probe locations) and circumventing deconvolution. The vertical position dependence of the NO signal has been used, however, to assess the local laser beam extinction by means of bidirectional laser scattering [15].

4.2. Attenuation effects

4.2.1. Brief summary of techniques

Previously, we have presented two combinations of techniques to assess the attenuation of both the laser beam and the ensuing NO fluorescence [15]. Here, we briefly summarise these techniques, including (1) bidirectional laser scattering (bidirectional LIF), (2) absorption spectroscopy of CO_2 and O_2, and (3) N_2 Raman scattering.

(1) With bidirectional LIF, spatial NO fluorescence intensity profiles are recorded from two counterpropagating laser pulses passing the same trajectory. From the ratio of these profiles, one can derive the (spatially resolved) laser beam attenuation [19–22].

(2) The detected NO LIF spectrum is affected by broadband UV absorption by CO_2 [23], which changes the relative intensities of the detected emission bands at 237, 248, 259, and 271 nm. Division of this LIF spectrum by a reference spectrum (i.e. without UV absorption) yields the *relative* transmission for each NO LIF band; *absolute* transmission values can be obtained by fitting the CO_2 transmission spectrum, using the parameterised CO_2 absorption cross section in Ref. [23]. This method is analogous to that of Hildenbrand and Schulz [24], who used O_2 LIF instead of NO LIF. Additionally, the NO fluorescence will suffer absorption by O_2. As the spectrally broad NO emission bands encompass many narrow O_2 absorption lines, the *effective* O_2 absorption can be *approximated* by a smooth, CO_2-like absorption function [25] (in our experiments leading to errors of $\leqslant 5\%$). It is fitted together with the CO_2 absorption spectrum.

By extrapolating the CO_2 absorption spectrum to 226 nm, it is possible to estimate the contribution of CO_2 absorption to the (total) laser beam extinction measured with bidirectional LIF (O_2 absorption is negligible as the laser beam is off O_2 resonance). The remaining extinction is attributed to absorption by NO and soot. The latter can be used to estimate the soot-based fluorescence attenuation.

(3) Provided the N_2 density is known, its Raman scattering signal reflects the combined transmission of the laser beam and the Raman-scattered light. N_2 density variations due to temperature inhomogeneities are corrected for using the estimated local temperature (see below). In our experiments, the Raman wavelengths are beyond the CO_2 and O_2 absorption ranges, and only the essentially wavelength-independent attenuation (attributed to soot) can be retrieved.

Since each of the abovementioned techniques only reveals a part of the attenuation, it is essential to combine the CO_2 and O_2 absorption spectra with either (1) bidirectional LIF or (2) N_2 Raman scattering results, to calculate the total attenuation of laser beam and fluorescence. These two strategies show good agreement [15]; their average is shown in Fig. 4 for both probe locations. It is evident that attenuation has a significant influence on the NO LIF signal, the combined transmission ranging between 1% and 90% during combustion. The earlier transmission decrease at the "through spray" location is caused by the fuel spray hitting the laser beam; the earlier increase is explained by the air swirl motion (clockwise in Fig. 1c and d), moving the flames and combustion products towards the "between sprays" position. (The curves in Fig. 4 are slightly different from the data in Ref. [26], where fluorescence attenuation by soot was not included.)

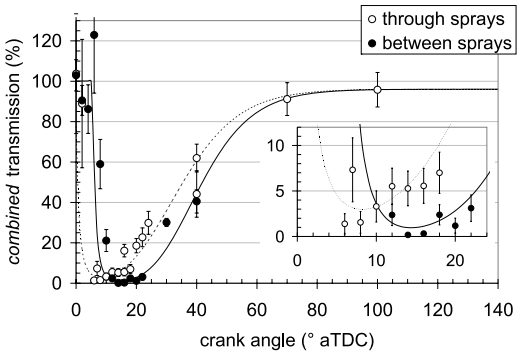

Fig. 4. Product of the laser beam transmission and the fluorescence transmission, for both probe positions. Lines to guide the eye.

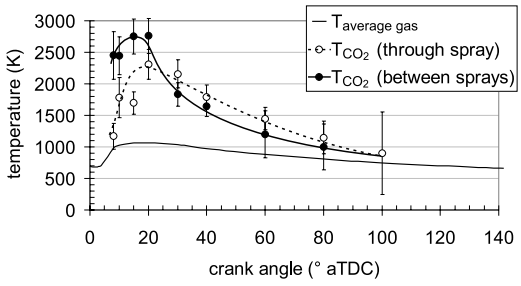

Fig. 5. "Local" effective temperatures estimated from fitted CO_2 and O_2 absorption spectra [25,15], and the average gas temperature during the combustion stroke. Lines through the data points guide the eye.

4.2.2. (Self) absorption by NO

At relatively high NO number densities ($\geqslant 2\times10^{17}$ cm^{-3}), laser beam attenuation due to NO absorption is no longer negligible. This means that the combined transmission (Fig. 4) and the NO density are essentially coupled. Self-consistent values for the NO density and combined transmission were obtained by iteratively calculating the transmission (including laser light absorption by NO) and the resulting NO number density, typically converging in 5–10 iterations. The effect of laser beam absorption by NO is included in Fig. 4.

Fluorescence trapping or self absorption by NO was not taken into account for two reasons. First, NO self-absorption spectra feature a much stronger wavelength and temperature dependence compared to CO_2, and do not match the observed relative LIF transmission. Second, since temperature variations along the absorption path are not accounted for (i.e. only one, effective, temperature is fitted), and due to the stronger temperature dependence of NO, the effective path length for NO absorption is expected to be considerably shorter than that for CO_2. This would result in less self-absorption than calculated from the *in situ* measurements.

4.3. NO LIF dependence on pressure, temperature, and gas composition

The pressure- and temperature-dependent terms in Eq. (1) require measurement of the pressure (Fig. 2) and the *local* temperature. The latter can be estimated from the measured CO_2 and O_2 absorption spectra (discussed in Section 4.2), taking advantage of their strong temperature dependence [23,27]. Since the CO_2 and O_2 absorption spectra are line-of-sight measurements, the fitted temperature is an effective temperature, biased to regions with strong absorption (i.e. high temperature and/or CO_2 density). However, it is arguably quite close to that in the probe volume, where we expect a temperature that is considerably higher (thus leading to stronger absorption) than in regions closer to the cylinder wall. The systematic temperature uncertainty due to this assumption is estimated at ~10%,[1] leading to ~5% uncertainty in the final NO density.

Figure 5 shows the estimated local temperature as well as the average gas temperature, derived from the pressure trace (assuming ideal gas behaviour and neglecting heat losses and blow-by) [28]. The local temperatures are substantially higher, especially between 10° and 60° aTDC, with peak temperatures around 2500 K at 20°–30° aTDC. Later in the stroke, they approach the average gas temperature. The difference between the two local temperatures before 20° aTDC might be explained by the presence of the evaporating fuel spray, extracting heat from its surroundings; shadowgraphy experiments showed a (liquid) spray structure until at least 7° aTDC [15]. Another possible explanation is the swirling air motion (clockwise in Fig. 1c), moving the hot combustion products from the "through spray" towards the "between sprays" position. After 60° aTDC, CO_2 and O_2 absorption becomes very small, causing an increased uncertainty of the fitted spectra and thus of the inferred temperature.

The calculated NO LIF variation due to the temperature and pressure variations during the stroke is shown in Fig. 6, for both constant ($[O_2]$:$[N_2] = 2$:8) and varying composition of the in-cylinder gases. The error bars are due to uncertainties in the measured temperature and pressure. For the varying gas composition we followed the approach of Van den Boom [29], who used mole

[1] This estimate is based on a number of calculations with several fictive temperature profiles along the NO fluorescence path. Each profile has a minimum at the detection window corresponding to the temperature of the unburnt gases and a maximum temperature at the probe volume. According to these calculations, the effective temperature is typically 10% lower than the maximum temperature.

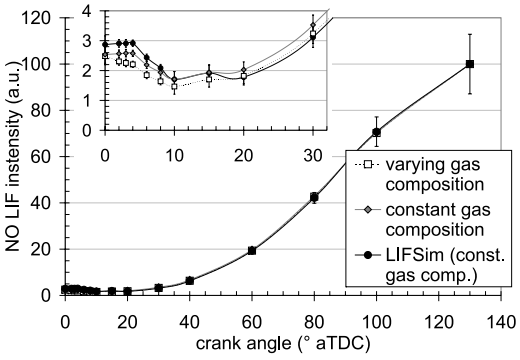

Fig. 6. Variation of the NO LIF intensity (per molecule) during the combustion stroke due to temperature and pressure. All curves are scaled to 100 at 130° aTDC. Input pressure and temperature are shown in Figs. 2 and 5, respectively.

fractions from gas sampling data by Aoyagi et al. [30] to estimate quenching rates for our engine. Our calculations show good agreement with the results from LIFSim [16], despite our assumption of temperature-independent quenching cross-sections [31]. Unfortunately, LIF*base* [32] does not calculate collisional quenching rates and thus cannot be used for comparison. The difference between constant and varying gas compositions is negligible compared to the experimental accuracy, except perhaps for crank angles <8° aTDC when they have the same order of magnitude. Further analysis is based on the LIFSim curve with constant gas composition.

5. Results and discussion

Figure 7 shows unprocessed, single-shot NO LIF measurements during the combustion stroke. The uncertainty in each data point is caused by camera noise (5% for crank angles ⩾15° aTDC). The large variation in single-shot NO LIF intensity (standard deviation ≈35%) is attributed to fluctuations in laser pulse energy (5%), and cycle-to-cycle variations of the engine. The latter include variations in NO number density, local temperature, and attenuation effects. The 15-shot average is included in Fig. 7, magnified by a factor of 10 to enhance the signal at early crank angles. At the "through spray" location NO molecules can be detected as early as 2° aTDC. The dip around 7° aTDC is due to attenuation effects: it resembles the combined transmission curve for this location (Fig. 4).

In the "between sprays" location, the earliest NO signal occurs at 8° aTDC, which is significantly later than in the fuel spray. Moreover, there is no pronounced attenuation-dip like in Fig. 7a, although the NO signal does level off between 10° and 20° aTDC. At 130° aTDC, both probe

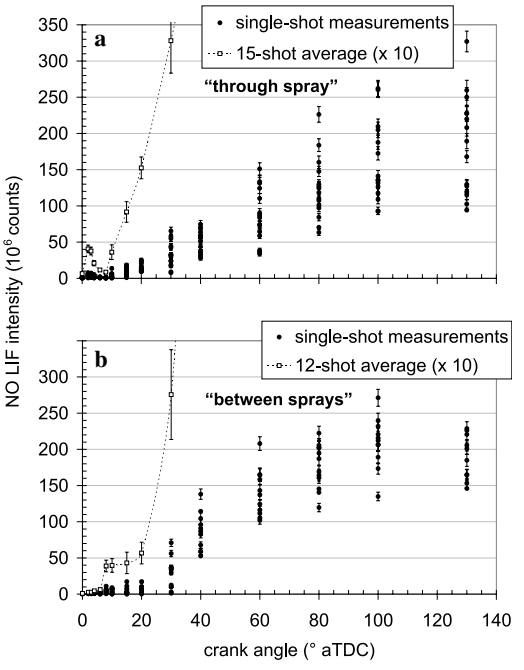

Fig. 7. Spatially averaged NO LIF intensity versus crank angle, for both probe positions. These (raw) data have not been processed for any pressure and temperature dependence of the LIF intensity, nor for attenuation effects. The single shot error bars denote the experimental accuracy; the error bars for the 15-shot average show the standard error of the average.

locations reach the same NO LIF intensity ("through spray": $(184 \pm 17) \times 10^6$ counts; "between sprays": $(189 \pm 9) \times 10^6$ counts), suggesting a uniform NO distribution at the end of the combustion stroke.[2] This is also reflected in (almost) uniform vertical NO LIF intensity profiles, see e.g. Fig. 3b. Uniform NO distributions late in the stroke have been reported before [3,33].

After processing the data in Fig. 7 for the pressure and temperature dependence of the NO fluorescence (Fig. 6) and for attenuation effects (Fig. 4), NO mole fractions are readily obtained. Window fouling effects (1% and 4% for "through spray" and "between spray", respectively [15]) are negligible compared to cycle-to-cycle variations. Subsequently, both curves are scaled at 130° aTDC to match the exhaust concentration (460 ± 30 ppm). The results are shown in Fig. 8. The error bars are primarily due to cycle-to-cycle variations and the attenuation correction; both yield relative standard errors around 10%, except early in the stroke when the latter has a 50% relative uncertainty (see Fig. 4). The large

[2] At 130° aTDC, temperature, pressure, and attenuation effects are equal for both locations.

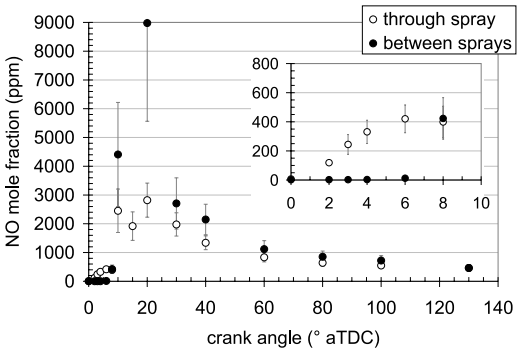

Fig. 8. Local NO concentrations during the combustion stroke. The data points are averages of 15 laser shots; the error bars denote the standard error (due to cycle-to-cycle variations of the NO concentration, the effective transmission, and of the local temperature).

"between sprays" concentrations and their errors at 15° and 20° aTDC are due to the large attenuation uncertainty at these crank angles, and not to the raw NO LIF signal as can be seen in Fig. 7b.

Interestingly, significant amounts of NO are present in the "through spray" location *before* the heat release rise at 3° aTDC. Moreover, the local temperature reaches 1800 K only around 10° aTDC. This indicates that the thermal (Zeldovich) mechanism for NO creation, requiring temperatures $\geqslant$1800 K, does not contribute to the early NO formation observed here. This is in contrast to the "between sprays" location, where the first detectable NO (8° aTDC, $T = 2450$ K) can be attributed to the thermal mechanism. However, it should be noted that the temperature measurements from CO_2 and O_2 absorption spectra are unlikely to resolve small, local combustion sites where temperatures may be sufficiently high to enable thermal NO formation. We have observed luminosity attributed to highly localised combustion spots already at 2–3° aTDC. Our findings of NO formation starting in, or even before, the premixed combustion phase (3–7° aTDC as estimated from Fig. 2) are in contrast to observations by Dec and Canaan [3], who concluded that NO is only created in the mixing-controlled combustion. This discrepancy might be related to attenuation effects, as Dec and Canaan used low-sooting fuels but did not mention corrections for additional attenuation by e.g. CO_2 absorption.

After 30° aTDC, both concentration curves are similar, and from 60° aTDC they decrease only very slowly to an asymptotic value of 460 ppm at 130° aTDC. The fact that the local NO concentration is virtually constant over the last 50° again indicates a homogeneous NO distribution in the measurement cylinder, as also found by Dec and Canaan [3], and by Corcione et al. [33]. This justifies our choice of calibration by the exhaust gas concentration. Interestingly, the NO concentration decreases by a factor of 5–10 during the later part of the combustion stroke. Although an initial "overshoot" around 20–30° aTDC has been observed [33,30] and predicted [34] for similar Diesel engines, the maximum is generally twice the concentration at the end of the stroke, or less. It should be noted, though, that those values are either cylinder averaged concentrations [33,34] or gas sampling data [30], whereas our probe volume is much more confined. This indicates the localised nature of the NO formation process: only 10–20% of the combustion chamber appears to be involved in the NO formation. Under the assumption that the *major* part of the total NO formed is due to the thermal mechanism, this conclusion is strengthened by the global temperature curve in Fig. 5 being much lower than the local ones.

6. Conclusions

Conversion of raw NO LIF signals into mole fractions requires knowledge of a number of conditions, such as cylinder pressure, the local temperature, and the attenuation of the light involved in the measurement. The latter can be measured using a combination of experimental techniques [15]. Despite the short path lengths involved in our setup, attenuation effects are considerable, and cannot simply be neglected.

The pressure and temperature dependence of the NO fluorescence leads to variations of over a factor of fifty during the combustion stroke. Optical transmission variations cover a similar range, so that the net post-processing factor for the LIF intensity varies over three orders of magnitude during an engine stroke. The error caused by the assumption of a constant gas composition is (much) less than the inaccuracy due to uncertainties in the local temperature (and pressure).

Our data provide evidence of highly localised NO formation processes, with peak values around 3000 ppm around 20° aTDC ("through spray"). The first NO signals occur during the premixed burn phase, in contrast to earlier observations by Dec and Canaan [3]. At this stage, the local temperature is still relatively low (<1800 K at 2–8° aTDC), indicating that the Zeldovich mechanism is not the only process responsible for NO formation. To verify this statement, the local temperature needs to be measured more accurately, and at better spatial resolution, e.g. by means of two-line vibrational thermometry [35].

Acknowledgments

This research is supported by the Technology Foundation STW, applied science division of

NWO and the technology programme of the Dutch Ministry of Economic Affairs.

References

[1] T.M. Brugman, R. Klein-Douwel, G. Huigen, E. van Walwijk, J.J. ter Meulen, *Appl. Phys. B* 57 (1993) 405–410.
[2] T.M. Brugman, G.G.M. Stoffels, N.J. Dam, W.L. Meerts, J.J. ter Meulen, *Appl. Phys. B* 64 (1997) 717–724.
[3] J.E. Dec, R.E. Canaan, SAE paper 980147 (1998).
[4] G.G.M. Stoffels, E.J. van den Boom, C.M.I. Spaanjaars, N. Dam, W.L. Meerts, J.J. ter Meulen, J.C.L. Duff, D.J. Rickeard, SAE paper 1999-01-1487, 1999.
[5] F. Hildenbrand, C. Schulz, J. Wolfrum, F. Keller, E. Wagner, *Proc. Combust. Inst.* 28 (2000) 1137–1143.
[6] E.J. van den Boom, P.B. Monkhouse, C.M.I. Spaanjaars, W.L. Meerts, N.J. Dam, J.J. ter Meulen, *Proc. SPIE* 4430 (2001) 593–606.
[7] F. Hildenbrand, C. Schulz, F. Keller, G. König, E. Wagner, SAE paper 2001-01-3500, 2001.
[8] P. Andresen, G. Meijer, H. Schlüter, et al., *Appl. Opt.* 29 (1990) 2392–2404.
[9] M. Knapp, A. Luczak, H. Schlüter, V. Beushausen, W. Hentschel, P. Andresen, *Appl. Opt.* 35 (1996) 4009–4017.
[10] F. Hildenbrand, C. Schulz, V. Sick, G. Josefsson, I. Magnusson, M. Aldén, SAE paper 980148, 1998.
[11] K. Akihama, T. Fujikawa, Y. Hattori, SAE paper 981430, 1998.
[12] F. Hildenbrand, C. Schulz, M. Hartmann, F. Puchner, G. Wawrschin, SAE paper 1999-01-3545, 1999.
[13] P. Jamette, V. Ricordeau, B. Deschamps, P. Desgroux, SAE paper 2001-01-1926, 2001.
[14] W.G. Bessler, M. Hoffmann, F. Zimmermann, et al., *Proc. Combust. Inst.* 30 (2005) 2667–2674.
[15] K. Verbiezen, R.J.H. Klein-Douwel, A.J. Donkerbroek, et al., *Appl. Phys. B* 83 (2006) 155–166.
[16] W.G. Bessler, C. Schulz, V. Sick, J.W. Daily, in: *Proceedings of the third Joint Meeting US Sec. Combust. Inst.*, Chicago, 2003, available at <http://www.lifsim.com>.
[17] N.M. Sijtsema, R.A.L. Tolboom, N.J. Dam, J.J. ter Meulen, *Opt. Lett.* 24 (1999) 664–666.
[18] R.A.L. Tolboom, N.J. Dam, J.J. ter Meulen, J.M. Mooij, J.D.M. Maassen, *Appl. Opt.* 43 (2004) 5669–5681.
[19] D. Stepowski, *Proc. Combust. Inst.* 23 (1990) 1839–1846.
[20] M. Versluis, N. Georgiev, L. Martinsson, M. Aldén, S. Kröll, *Appl. Phys. B* 65 (1997) 411–417.
[21] G.G.M. Stoffels, S. Stoks, N. Dam, J.J. ter Meulen, *Appl. Opt.* 39 (2000) 5547–5559.
[22] V. Sick, B.D. Stojkovic, *Appl. Opt.* 40 (2001) 2435–2442.
[23] C. Schulz, J.B. Jeffries, D.F. Davidson, J.D. Koch, R.K. Hanson, *Proc. Combust. Inst.* 29 (2002) 2735–2742.
[24] F. Hildenbrand, C. Schulz, *Appl. Phys. B* 73 (2001) 173–180.
[25] K. Verbiezen, A.P. van Vliet, W.L. Meerts, N.J. Dam, J.J. ter Meulen, *Combust. Flame* 144 (2005) 638–641.
[26] K. Verbiezen, A.P. 'van Vliet, R.J.H. Klein-Douwel, et al., in: Proc. Europ. Combust. Meeting 2005, Louvain-la-Neuve, Belgium, 2005.
[27] J.B. Jeffries, C. Schulz, D.W. Mattison, et al., *Proc. Combust. Inst.* 30 (2005) 1591–1599.
[28] J.B. Heywood, *Internal Combustion Engine Fundamentals*, McGraw-Hill, Singapore, 1988.
[29] H.L.G.J. van den Boom, *Laser diagnostics in diesel engines*, Ph.D. thesis, University of Nijmegen, 2000.
[30] Y. Aoyagi, T. Kamimoto, Y. Matsui, S. Matsuoka, SAE paper 800254, 1980.
[31] P.H. Paul, J.A. Gray, J.J.L. Durant, J.J.W. Thoman, *Chem. Phys. Lett.* 57 (1993) 249–259.
[32] J. Luque, D.R. Crosley, Report MP 99-009, SRI International, 1999.
[33] F.E. Corcione, S.S. Merola, B.M. Vaglieco, SAE paper 2002-01-0892, 2002.
[34] H. Barths, C. Antoni, N. Peters, SAE paper 982459, 1998.
[35] W.G. Bessler, F. Hildenbrand, C. Schulz, *Appl. Opt.* 40 (2001) 748–756.

Comments

Christof Schulz, University of Duisburg-Essen, Germany. The calibration of your LIF-based NO-concentration measurements relies entirely on a comparison of in-cylinder measurements late in the cycle and exhaust-gas analysis. Because in the inhomogeneous distribution of NO in the cylinder, however, volume-averaging exhaust-gas measurements often show lower values than optical measurements within the combustion region around the diesel sprays. What is the error evolving from this calibration strategy?

Reply. Our data show that the NO concentration is virtually constant for more than 8 ms, which leaves plenty of time for further mixing with unburned air or combustion products. The fact that this mixing does not affect the measured local NO concentration indicates that the cylinder contents is already reasonably homogeneous. The two probe locations reaching the same asymptotic NO concentration is a further proof of this. As is mentioned in Section 5, homogeneous NO concentrations near the end of the stroke have also been observed by Dec and Canaan ([3] in paper) and by Corcione et al. ([33] in paper).

•

Alan Eckbreth, Consultant, USA. In your work, there seems to be an absence of fluorescent interferences which seems surprising given excitation near 226 nm. To what do you attribute the lack of interferences, e.g., positioning in cylinder, crank angle position, etc.?

Reply. The $A^2\Sigma(v' = 0)$—$X^2\Pi(v'' = 0)$ transitions near 226.03 nm are very popular for their low-level of O_2 LIF interference, as was presented by DiRosa et al. [1]. Indeed, Fig. 3 shows that our data are free of any O_2 fluorescence. This was the case for both probe locations. We did not use any special "tricks" to suppress the O_2 LIF. We did observe Raman scattering by O_2 and N_2 early in the stroke.

Reference

[1] M.D. DiRosa, K.G. Klavuhn, R.K. Hanson, *Combust. Sci. Tech.* 118 (1996) 257–283.

●

Katharina Kohse-Höinghaus, Universität Bielefeld, Germany. Is it correct that you use the same information to infer the temperature and the transmission correction? This could be interdependent and influence your error estimate.

Reply. As is detailed in ([25] in paper), the changes in relative intensities of the four NO fluorescence bands during the stroke can be attributed to UV absorption by hot CO_2 and O_2. We fit their parameterized absorption cross-sections $\sigma(\lambda, T)$ to obtain absolute transmission values (by dividing the peak intensities by a reference spectrum, one obtains only the relative fluorescence transmission). These absolute transmission values are used (a.o.) to correct for attenuation effects. At the same time, one of the fit parameters, T, is used later to process the NO LIF data for the temperature dependence of the fluorescence yield.

In principle, fitting a "wrong" temperature might lead to errors in the attenuation correction. In practice, this would be compensated to some extent by the other fit parameter, the CO_2 number density. Concerning the error estimate, both the temperature error and the attenuation correction error were calculated from the uncertainties in the NO LIF peak ratios. The calculation of the temperature uncertainty does not depend on the calculation of the attenuation uncertainty, or vice versa.

●

Thomas B Settersten, Sandia National Laboratories, USA. You have indicated that LIFSIM was used to correct your images for the effect of collisional quenching on the measured signals. The calculation of quenching rates requires specification of the local temperature, pressure, and composition, and quenching rates can vary dramatically with changes in the collisional conditions. Can you please elaborate on your estimation of the collisional environment and the significance of the quenching corrections?

Reply. We use the corrections for attenuation and the dependence of the LIF yield on pressure and temperature to arrive at relative concentration histories during the stroke. Absolute concentration values are obtained after calibration. The quenching rate strongly depends on both the cylinder pressure and the gas composition: the quenching cross-section varies from species to species. Here, only the relative change of the quenching rate is of importance, and it depends mainly on pressure rather than on the exact gas composition, as is shown in Fig. 6. In terms of absolute quenching rates, there is, of course, a large difference between the curves for varying and constant gas composition, as the quenching cross-section of N_2 is relatively low.

●

Jay Jeffries, Stanford University, USA. The broadband background (presumably from CO_2) should vary with crank angle. How does this background vary and what fraction of the total signal is the largest background?

Reply. Although CO_2 is known to fluoresce (and absorb) in the NO LIF spectral region, fuel LIF and soot (laser-induced) incandescence are other possible contributors to the total background, as well as dark current from the CCD camera. When making cross-sections of the NO LIF images like those in Fig. 3, the background showed no structure, nor any wavelength dependence, for any of the crank angles in Fig. 7. Estimating the dark current from measurements before the start of combustion, the remaining background is found to be minimal, increasing from virtually zero to less than 25% of the total background intensity at the end of the stroke. Since also this background shows no structure, it is attributed to straylight in the spectrograph system. No attempts were made to further identify its origin.

The background fraction of the total signal varies during the stroke. At 130° aTDC, when the LIF intensity is highest, the background (including dark current) is 5% of the total. At 20° aTDC (maximum NO concentration, but low fluorescence intensity), it is 35%.